# Microsolvation of the Water Cation in Argon: II. Infrared Photodissociation Spectra of $H_2O^+-Ar_n$ ($n = 1-14$)

## Otto Dopfer,* Doris Roth, and John P. Maier

*Institut für Physikalische Chemie, Universität Basel, Klingelbergstrasse 80, CH-4056 Basel, Switzerland*

*Received: July 12, 2000; In Final Form: September 25, 2000*

Mid-infrared photodissociation spectra of $H_2O^+-Ar_n$ ($n = 1-14$) complexes have been recorded in the vicinity of the O−H stretch vibrations of the water cation. The rovibrational structure of the transitions in the dimer spectrum ($n = 1$) are consistent with a planar, proton (H)-bound H−O−H−Ar equilibrium geometry. The slightly translinear intermolecular bond in the ground vibrational state is characterized by a bond angle $\varphi_0 = 175(5)°$, an interatomic H−Ar separation $R_0 = 1.929(15)$ Å, and an intermolecular stretching force constant $k_s \sim 29$ N/m. The assignment of the vibrational transitions is confirmed by spectra of partly deuterated species. The relaxation dynamics depend strongly on the excited vibrational state and do not obey statistical theories. Analysis of the spin-rotation constants indicates that the electromagnetic properties of the $H_2O^+$ cation in its $^2B_1$ ground electronic state are not significantly affected by the formation of the intermolecular bond to Ar. The vibrational bands in the spectra of larger clusters ($n = 2-14$) are assigned to O−H stretch fundamentals and their combination bands with the intermolecular H−Ar stretch modes. The observed systematic band shifts as a function of cluster size provide information about the cluster's geometries and the occurrence of structural isomers. The most stable trimer ($n = 2$) geometry has two equivalent intermolecular H-bonds. This stable trimer core is further solvated by two Ar ligands attached to opposite sites of the $2p_y$ orbital of oxygen ($n = 3,4$) and subsequently by less strongly bound Ar ligands ($n = 5-14$) to form an Ar solvation shell, probably around an interior $H_2O^+$ ion.

## I. Introduction

Ion−ligand interactions are of fundamental importance for many processes in physics, chemistry, and biology.[1,2] To understand these phenomena from the microscopic point of view, detailed knowledge of the interaction potential between the ion ($A^\pm$) and the surrounding ligands (L) is required. Ionic complexes ($A^\pm-L_n$) isolated in the gas phase are attractive model systems to investigate ion−ligand potentials both experimentally and theoretically. Mass spectrometric studies have resulted in the determination of ion−ligand binding energies for a vast number of $A^\pm-L_n$ combinations and provided some insight into the cluster growth process (i.e., the closure of solvation shells via the observation of magic numbers).[3−5] However, these studies are not sensitive to the details of the potential energy surface (PES). During the past 15−20 years, the combination of high-resolution spectroscopy and quantum chemical calculations has provided a more sensitive probe of the detailed shape of PESs in ionic complexes.[6−11]

The present work reports IR spectra of mass selected $H_2O^+-Ar_n$ ($n = 1-14$) complexes to investigate the $H_2O^+-Ar$ interaction and the stepwise microsolvation process of the water cation in argon. The experimental approach is complemented by ab initio calculations for the smaller species ($n = 0-4$), the results of which are discussed in detail in the preceding paper (henceforth referred to as article I).[12] Similar theoretical and experimental studies have previously been reported for related $AH^+-Ar_n$ complexes, including A = CO ($n = 1-13$),[13] $N_2$ ($n = 1-13$),[14] SiO ($n = 1-10$),[15] $CH_2$ ($n = 1-8$),[16] and $NH_3$ ($n = 1-7$).[17−20] In all these cases, rotationally resolved spectra

have been observed for the dimers ($n = 1$), the analysis of which provided information about details of the intermolecular potential (e.g., structure, binding energy, intermolecular stretching and bending force constants, nonrigidity, barriers for internal motions). For larger complexes ($n \geq 2$), usually only spectra at the level of vibrational resolution have been obtained. Nonetheless, the observed systematic shifts in vibrational frequencies as a function of cluster size, as well as the analysis of photofragmentation branching ratios, provided useful information about the cluster growth (e.g., structures, binding energies, closure of solvation shells, occurrence and stability of different isomers).

The $H_2O^+-Ar_n$ series differs in several aspects from the previously studied $AH^+-Ar_n$ systems. (1) $H_2O^+$ is a bent dihydride cation, that is, $H_2O^+-Ar_n$ represents a prototype for $AH_2^+-Ar_n$ systems having the possibility of forming two proton bonds.[12] The analysis of the spectra reveals that this property significantly influences the cluster growth, which largely differs from that of $AH_k^+-Ar_n$ with $k \neq 2$. For example, $AH^+-Ar_n$ systems with linear closed-shell triatomic cores ($AH^+ = OCH^+$, $N_2H^+$, $SiOH^+$) have icosahedral-like structures with first solvation shell closure at $n = 12$.[13−15] In contrast, mass spectra of $H_2O^+-Ar_n$ feature magic numbers at $n = 3, 5, 7, 9,$ and 15 (but not at $n = 12$), indicating that the cluster structures must deviate significantly from icosahedral-like geometries.[21] (2) As a consequence of the large spin-rotation interaction of $H_2O^+$ in its $^2B_1$ electronic ground state,[22] the $H_2O^+-Ar$ dimer is the first ionic complex for which the spin-rotation splitting is resolved. In addition to the rotational constants, the change in the spin−rotation constants upon Ar complexation provides valuable information about the dimer geometry and the influence of Ar

---

* Corresponding author. E-mail: otto.dopfer@unibas.ch.

IR Photodissociation Spectra of H₂O⁺−Ar_n

*J. Phys. Chem. A, Vol. 104, No. 50, 2000* **11703**

complexation on the electromagnetic properties of the electronic ground state of $H_2O^+$. So far, the only ionic open-shell complexes, for which fine structure caused by electron spin have been resolved in IR spectra, are the linear proton (H)-bound $OH^+-He/Ne$[23] and $HNH^+-He/Ar$ dimers,[24,25] which all has $^3\Sigma^-$ electronic ground states. (3) Most of the $AH^+-Ar$ dimers (e.g., A = CO, $N_2$, SiO, NH, OCO, HCl) possess strongly directional (near) linear H-bonds.[13–15,24,26,27] The $H_2O^+$ cation has a partially filled $2p_y$ orbital at oxygen, which can act as electron acceptor and stabilize via partial charge transfer from Ar to $H_2O^+$ a p-bound $H_2O^+-Ar$ structure (in which the Ar is attached in a T-shaped fashion to the $2p_y$ orbital). Although ab initio calculations predict the H-bound minimum of $H_2O^+-Ar$ to be lower in energy than the p-bound minimum,[12] it was hoped to observe the p-bound structure in the present experiment. In addition, the existence of two different competing minima on the dimer PES was expected to have strong influence on the cluster growth.

The water cation, which serves as the IR chromophore in the $H_2O^+-Ar_n$ complexes, is an important ion in the ion–molecule reaction chemistry of water-containing plasmas, planetary atmospheres, and interstellar media.[28,29] The $^2B_1$ ground electronic state of $H_2O^+$ has been characterized in the gas phase by photoelectron spectroscopy[30–33] and high-resolution rotational,[34–36] rovibrational,[37–39] and rovibronic spectroscopy.[22,40,41] Neon matrix isolation studies yielded the missing fundamental frequencies of all H/D isotopomers.[42] In addition, ab initio calculations at various levels of theory have been applied to $H_2O^+$,[43–50] and the recent study by Brommer et al.[49] reproduces the experimental data to high accuracy. The properties of $H_2O^+$ and its isotopomers relevant to the present study are summarized in Tables 1 and 2 of article I.[12]

Complexes of $H_2O^+$ with $Ar$[21,51,52] and various closed-shell molecular ligands[28,29] have been identified in mass spectrometric experiments. Some of them correspond to collisionally stabilized intermediates of chemical reactions. However, no spectral data seem to exist on $H_2O^+-L$ complexes, except low-resolution photoelectron spectra.[53,54] Hence, the spectrum of $H_2O^+-Ar$ presented in the present work provides the first high-resolution spectroscopic information about structure and stability of $H_2O^+-L$ dimers. The article is organized in the following way: after describing the experimental procedure, the results are separately discussed for $H_2O^+-Ar_n$ with $n = 1, 2,$ and $3-14$ in strong conjunction with the ab initio calculations presented in article I.[12]

## II. Experimental Section

Mid-IR photodissociation spectra of $H_2O^+-Ar_n$ are recorded in a tandem mass spectrometer apparatus described elsewhere.[8,13] The complexes are produced in a cluster ion source that combines a supersonic expansion with electron impact ionization. Argon is bubbled at a stagnation pressure of 5−15 bar and room temperature through a reservoir filled with distilled water, and the resulting vapor is expanded through a pulsed nozzle (Ø 1 mm). A 1:1 mixture of $H_2O$ and $D_2O$ is used for the production of $HDO^+-Ar_n$. Close to the nozzle orifice the expansion is crossed by two electron beams (kinetic energy ∼100 eV) emitted from heated tungsten filaments. Electron impact ionization of the gas mixture is followed by ion–molecule and clustering reactions to form a variety of (cluster) ions. A typical mass spectrum of the ion source (Figure 1) is composed mainly of the series $Ar_n^+$, $H^+-Ar_n$, $H_2O^+-Ar_n$, $H_3O^+-Ar_n$, and $H_3O^+-(H_2O)_n$. The dimerization efficiency, $I_{H_2O^+-Ar}/I_{H_2O^+}$, is about 10%. Several other gas mixtures
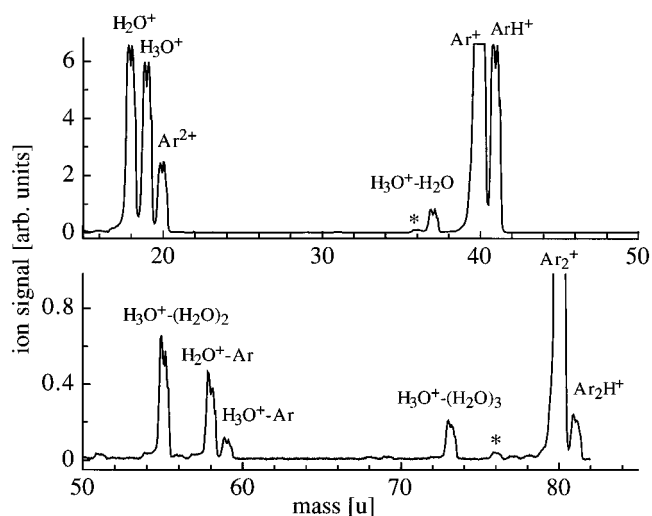


**Figure 1.** Mass spectrum of the cluster ion source in the range 15−85 u for the expansion of the $H_2O/Ar$ mixture. The $Ar^+$ peak is saturated. The spectrum is dominated by the cluster ion series $Ar_n^+$, $H^+-Ar_n$, $H_2O^+-Ar_n$, $H_3O^+-Ar_n$, and $H_3O^+-(H_2O)_n$. The dimerization efficiency, $I_{H_2O^+-Ar}/I_{H_2O^+}$, is of the order of 10%. Asterisks indicate the occurrence of unprotonated $(H_2O)_m^+-Ar_n$ clusters.

containing $H_2$, $O_2$, He, and Ar in a broad range of mixing ratios and backing pressures are tried as well; however, the $H_2O^+-Ar_n$ currents achieved are in all cases lower than those of the $Ar/H_2O$ mixture. Small currents of unprotonated $(H_2O)_m^+-Ar_n$ clusters are also observed (marked by asterisks in Figure 1), presumably through ionization of larger neutral $(H_2O)_m-Ar_k$ complexes $(k > n)$ and subsequent cooling by evaporation of Ar ligands.[51,52]

Part of the plasma created in the ion source is extracted through a skimmer (Ø 1 mm) into a first quadrupole mass spectrometer (QMS), which is tuned to the mass of $H_2O^+-Ar_n$. The mass selected parent beam is then focused into an octopole ion guide, where it overlaps with the counter propagating IR laser pulse. Resonant absorption of $H_2O^+-Ar_n$ in the mid-IR spectral range leads to the excitation of rovibrational levels above the lowest dissociation limit and subsequent fragmentation into $H_2O^+-Ar_m$ and $(n-m)$ Ar atoms. The $H_2O^+-Ar_m$ fragment ions are selected by a second QMS located after the octopole and directed onto a Daly ion detector coupled to a boxcar integrator. A photodissociation spectrum of the parent cluster ion is obtained by monitoring the fragment ion current as a function of the IR laser frequency. To separate the contribution of fragment ions caused by laser-induced dissociation from the background signal, which mainly originates from metastable decomposition of hot parent clusters and collision-induced dissociation in the octopole region, the ion source is triggered at twice the laser frequency, and the signal acquired with the laser off is subtracted from that with the laser on. This procedure is less important for cluster sizes with $n \geq 4$, because these evaporate more than one Ar ligand upon mid-IR excitation. Metastable decay and collision-induced dissociation processes lead almost exclusively to the production of $m = n - 1$ fragment ions, that is, they interfere with the laser-induced dissociation signals only for small cluster sizes $(n \leq 3)$. All photofragmentation spectra are normalized for variations in the IR intensity measured with an InSb detector.

Pulsed and tunable IR radiation with a bandwidth of 0.02 cm⁻¹ is produced by a seeded Nd:YAG pumped single-mode optical parametric oscillator (OPO) laser system operating at 20 Hz (tuning range 2500−6800 cm⁻¹). The laser frequency
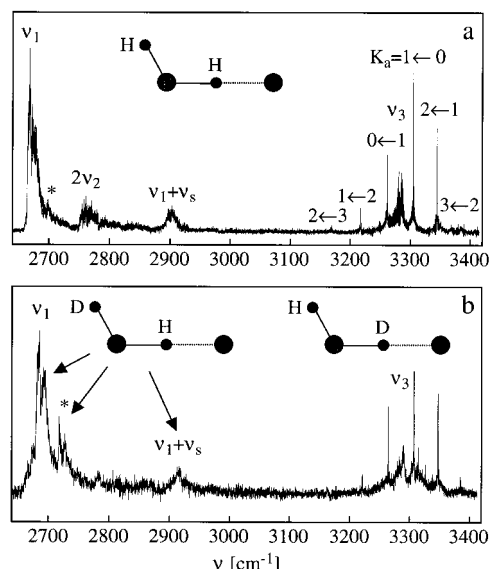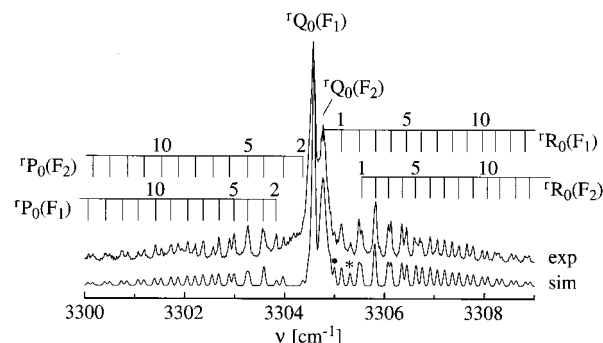
**Figure 2.** Mid-IR photofragmentation spectra of $H_2O^+-Ar$ (a) and $HDO^+-Ar$ (b) with assignments. As the spectra are composed of several shorter scans recorded separately, only the relative intensities of closely spaced transitions are reliable. The weak signal in the blue wing of $\nu_1$ is attributed to sequence bands, $\nu_1 + \nu_x \leftarrow \nu_x$, where $\nu_x$ are intermolecular modes. The P branch heads marked by asterisks are assigned to $\nu_1 + \nu_s \leftarrow \nu_s$. In the $HDO^+-Ar$ spectrum, transitions of both possible isotopomers, $HOD^+-Ar$ and $DOH^+-Ar$, are identified.



**Figure 3.** The $K_a = 1 \leftarrow 0$ subband of the $\nu_3$ transition of $HOH^+-Ar$ along with assignments and a simulation based on the molecular constants in Table 1, a bimodal Boltzmann distribution with $T = 6.8$ and 18.3 K with equal weight, and a convolution width of 0.06 cm$^{-1}$. The forbidden $^rR_0(0)$ $F_2 \leftarrow F_1$ and allowed $^rQ_0(1)$ $F_2$ lines are indicated by an asterisk and a filled circle, respectively. The spin-rotation splitting $(F_1/F_2)$ decreases with increasing $N$ in both P and R branches.

is calibrated by optoacoustic reference spectra[55] of $NH_3$, HDO, and $C_2H_2$ recorded with either the signal or idler outputs of the OPO, and interpolation is facilitated by transmission étalon fringes of the OPO oscillator. The calibrated rotational line positions of the $H_2O^+-Ar$ ($HDO^+-Ar$) dimer are corrected for the Doppler shift induced by the kinetic energy of the ions in the octopole, $E_{kin} = 5.5 \pm 1$ eV. The absolute accuracy of rotational line positions is limited to $\pm 0.02$ cm$^{-1}$ by a combination of the laser bandwidth (0.02 cm$^{-1}$) and the uncertainty in the kinetic energy of the ions. The Doppler width, estimated as <0.005 cm$^{-1}$ for the dimer, provides only a minor contribution to the instrumental line width. For rotationally resolved transitions at least three scans are recorded, and the extracted rotational line positions are averaged over the individual scans.

### III. Results and Discussion

**A. $H_2O^+-Ar$ dimer ($n = 1$). *1. Vibrational analysis*.** Figure 2a shows the mid-IR photodissociation spectrum of $H_2O^+-Ar$ recorded between 2630 and 3410 cm$^{-1}$. Four bands centered at 2672, 2767, 2905, and 3284 cm$^{-1}$ are assigned to the $\nu_1$, $2\nu_2$, $\nu_1 + \nu_s$, and $\nu_3$ transitions of a H-bound $HOH^+-Ar$ dimer based on their frequencies, isotopic shifts, IR intensities, and rotational structure. The assignments are also supported by the results of ab initio calculations described in article I.[12] The reader is referred to Figures 1 and 3 of article I for the calculated structure and normal coordinates of the H-bound dimer.[12] If not stated otherwise, the experimental data for the dimers ($n = 1$) are compared to the ab initio results obtained at the MP2/aug-cc-pVTZ$^{\#}$ level.

The intense unresolved transition at 2672 cm$^{-1}$ is attributed to the $\nu_1$ fundamental of $HOH^+-Ar$, which corresponds to the bound O—H stretch. The large observed red shift ($\Delta\nu_1 = -541$ cm$^{-1}$) from the monomer value ($\nu_1 = 3212.9$ cm$^{-1}$)[39] is somewhat larger than the predicted shift ($\Delta\nu_1 = -477$ cm$^{-1}$),[12] as the calculations underestimate the large anharmonicity of the

proton motion along the proton-transfer coordinate. The calculated equilibrium structure of the H-bound $HOH^+-Ar$ dimer is very close to a prolate symmetric top ($\kappa_e = -0.99989$) with the $a$-axis almost parallel to the intermolecular bond.[12] Consequently, the transition dipole moment of the $\nu_1$ fundamental lies nearly parallel to the $a$-axis giving rise to a hybrid band with an intense parallel ($\Delta K_a = 0$) and a very weak perpendicular ($\Delta K_a = \pm 1$) component. Assuming that the $\nu_1$ mode is a pure O—H donor stretch, the intensity ratio between both components is estimated as ~200. Indeed, the band shape of the $\nu_1$ transition is characteristic of a pure parallel transition with overlapping $\Delta K_a = 0$ subbands, leading to the coarse appearance of single P, Q, and R branches. The observed sharp P branch head indicates that the intermolecular separation decreases upon $\nu_1$ excitation. Further analysis of the $\nu_1$ band contour is presented in section III.A.3.

A weaker unresolved band centered at $2904.5 \pm 1$ cm$^{-1}$ is interpreted as the $\nu_1 + \nu_s$ combination band, giving rise to an intermolecular stretching frequency in the $\nu_1$ state, $\nu_s = 232.3 \pm 1$ cm$^{-1}$. Similar to the $\nu_1$ fundamental, the transition dipole moment of the $\nu_1 + \nu_s$ vibration lies nearly parallel to the $a$-axis of the complex, leading to the appearance of a parallel band. Weak signals in the blue wing of the $\nu_1$ band are attributed to sequence transitions of the type $\nu_1 + \nu_x \leftarrow \nu_x$, where $\nu_x$ are intermolecular vibrations. Such transitions were previously observed in related H-bound ionic complexes.[15,24,26] The strongest of them with a strong P branch head has a band origin at $2705 \pm 2$ cm$^{-1}$ and is attributed tentatively to the $\nu_1 + \nu_s \leftarrow \nu_s$ transition (indicated by an asterisk in Figure 2a). Combining this value with the $\nu_1 + \nu_s$ position gives rise to a ground-state intermolecular stretching frequency, $\nu_s = 200$ cm$^{-1}$, in close agreement with the calculated value, $\nu_s = 207$ cm$^{-1}$.[12] Approximating $H_2O^+-Ar$ as a diatom, the force constant for the intermolecular bond can be estimated as $k_s \sim 29$ N/m. A further broad and unresolved transition centered at $2767 \pm 5$ cm$^{-1}$ is assigned to the first overtone of the $\nu_2$ vibration of the dimer ($\nu_2$ is the intramolecular H—O—H bend). The small red shift of $\Delta 2\nu_2 = -4$ cm$^{-1}$ from the monomer value, $2\nu_2 = 2771.3$ cm$^{-1}$,[38] compares favorably with the harmonic ab initio prediction of $-5$ cm$^{-1}$.[12]

The intense transition centered at 3284 cm$^{-1}$ is assigned to the $\nu_3$ fundamental, which corresponds to the free O—H stretch vibration of $HOH^+-Ar$. Consequently, its transition moment has both large perpendicular and parallel components giving rise to the observed hybrid band. Assuming that the transition

dipole lies along the free O—H bond of the calculated dimer geometry,[12] the intensity ratio between perpendicular and parallel components is estimated as ~5, in qualitative agreement with the experimental observation (~2). The observed complexation induced blue shift, $\Delta\nu_3 = 25$ cm$^{-1}$, is comparable with the calculated value, $\Delta\nu_3 = 17$ cm$^{-1}$.[12] A blue shift of similar magnitude (~20 cm$^{-1}$) has been observed recently for the free Cl—H stretch fundamental of the related H-bound HClH$^+$—Ar dimer.[27]

The vibrational assignments of the $H_2O^+$—Ar bands are supported by the corresponding spectrum of the complex with HDO$^+$ (Figure 2b). In the latter dimer, two structural isomers may exist: the Ar atom can bind either to the H or D atom of HDO$^+$ to form either HOD$^+$—Ar or DOH$^+$—Ar. Vibrational analysis of the spectrum in Figure 2b clearly reveals the presence of both isomers in the expansion. The spectral fingerprints of DOH$^+$—Ar are considered first. The bound O—H stretch vibration of DOH$^+$—Ar (denoted $\nu_1$) occurs at $2688.5 \pm 1$ cm$^{-1}$ and is shifted 16 cm$^{-1}$ to higher frequency than HOH$^+$—Ar. The ab initio calculations predict a significantly smaller blue shift of ~1 cm$^{-1}$,[12] indicating that the harmonic approach (with subsequent scaling) is certainly not sufficient to accurately predict the shift of this highly anharmonic vibration upon deuteration of the free O—H bond. The $\nu_1 + \nu_s$ combination and $\nu_1 + \nu_s \leftarrow \nu_s$ sequence bands are observed at $2918 \pm 2$ and $2724 \pm 1$ cm$^{-1}$, implying $\nu_s = 194$ and $229$ cm$^{-1}$ in the ground and $\nu_1$ vibrational states. They are lower than those of HOH$^+$—Ar (200 and 232 cm$^{-1}$) owing to the 4% decrease of the reduced mass upon deuteration (treating the dimer as a diatom). Calculations predict that deuteration of the dangling proton shifts the free O—D stretch ($\nu_3 = 2369$ cm$^{-1}$) and $\nu_2$ overtone ($2\nu_2 \sim 2490$ cm$^{-1}$) of DOH$^+$—Ar out of the scanning range of the OPO (>2500 cm$^{-1}$).[12] Consequently, they are not observed in the spectrum of Figure 2b. Similarly, deuteration of the donating proton shifts the bound O—D stretch ($\nu_1 = 1990$ cm$^{-1}$) and $2\nu_2$ (~2364 cm$^{-1}$) of the second isotopomer, HOD$^+$—Ar, out of the investigated spectral range.[12] However, the free O—H stretch fundamental is observed at ~3286.5 cm$^{-1}$, and the small observed shift upon deuteration (~2.5 cm$^{-1}$) is consistent with the theoretical prediction ($-0.4$ cm$^{-1}$).

All vibrational features in the spectra of $H_2O^+$—Ar and HDO$^+$—Ar in Figure 2 are attributed to the H-bound structure, which is calculated to be the global minimum on the PES. There is no spectral signature of a less stable p-bound dimer which is predicted to be a local minimum.[12] The small population of this local minimum under the present experimental conditions may either be due to a significantly lower binding energy or a small barrier for isomerization to the H-bound global minimum.

*2. Rotational Analysis.* In contrast to all other observed bands, the $\nu_3$ hybrid transition of the $H_2O^+$—Ar dimer displays rotational resolution. Adjacent unresolved Q branches of $\Delta K_a = \pm 1$ subbands of the perpendicular component are separated by $2(A'-B')\sim 40$ cm$^{-1}$ (Figure 2a), and the overlapping $\Delta K_a = 0$ subbands of the parallel component appear between the $K_a = 1 \leftarrow 0$ and $0 \leftarrow 1$ subbands. The Hamiltonian used for the analysis contains terms for the vibrational and rotational motions as well as the spin-rotation interaction:

$$\hat{H} = \hat{H}_{vib} + \hat{H}_{rot} + \hat{H}_{sr} \qquad (1)$$

The vibrational Hamiltonian, $\hat{H}_{vib}$, gives rise to the band origin, $\nu_0$. For the rotational structure, a standard semirigid prolate symmetric top Hamiltonian including quartic centrifugal distortion terms is used[56]:

$$\hat{H}_{rot} = \bar{B}\hat{N}^2 + (A - \bar{B})\hat{N}_z^2 \pm (C - B)\hat{N}^2 \delta_{K_a1} - D_N\hat{N}^4 -$$
$$D_{NK}\hat{N}^2\hat{N}_z^2 - D_K\hat{N}_z^4 \quad (2)$$

The term $(C - B)\hat{N}^2\delta_{k_a1}$ accounts for the small but resolved asymmetry splitting of each rotational level in the $K_a = 1$ state into the $c$ and $d$ parity doublets arising from $B - C \sim 0.0013$ cm$^{-1}$ ($\delta_{K_a1} = 1$ for $K_a = 1$ and $\delta_{K_a1} = 0$ otherwise), and $\bar{B} = (B + C)/2$. Because the asymmetry parameter $\kappa$ is very close to $-1$, the asymmetry splitting is only resolved for $K_a = 1$ at the present spectral resolution.[56] The Hamiltonian used for the description of the spin-rotation interaction in the $^2A''$ electronic state of HOH$^+$—Ar is appropriate for symmetric tops in doublet electronic states[57]:

$$\hat{H}_{sr} = a_0(\hat{N}_x\hat{S}_x + \hat{N}_y\hat{S}_y + \hat{N}_z\hat{S}_z) + a(2\hat{N}_z\hat{S}_z - \hat{N}_x\hat{S}_x - \hat{N}_y\hat{S}_y)$$
$$(3)$$

According to Hund's case (b), the electron spin, $\hat{S}$, couples with the rotational momentum, $\hat{N}$, to form the total angular momentum, $\hat{J} = \hat{N} + \hat{S}$. Thus, in a doublet electronic state ($S = 1/2$) each rotational level with $N \geq 1$ is split into two components by the spin-rotation interaction with total angular momentum $J = N + 1/2$ ($F_1$) and $N - 1/2$ ($F_2$), respectively. The selection rules for allowed transitions are $F_i \leftarrow F_i$ ($i = 1,2$), $\Delta J = 0, \pm 1$, and $\Delta J = \Delta N$. Additional selection rules for the parallel $a$—type band are $\Delta K_a = 0$, $+ + \leftrightarrow - +$, and $+ - \leftrightarrow - -$, whereas transitions in the perpendicular $b$—type band connect levels with $\Delta K_a = \pm 1$, $+ + \leftrightarrow - -$, and $+ - \leftrightarrow - +$, respectively.[56]

In total, 729 P and R branch transitions in the parallel and perpendicular components of $\nu_3$ are assigned (see Figures 3 and 4 for the $K_a = 1 \leftarrow 0$ and $K_a = 2 \leftarrow 1$ subbands: $^{\Delta K_a}\Delta N_{K_a}(N)$ = $^rP_1(4-13)$, $^rR_1(1-21)$, $^rP_0(2-16)$, $^rR_0(1-13)$, $^pP_1(2-38)$, $^pR_1(1-21)$, $^pP_2(2-21)$, $^pR_2(2-6)$, $^qP_0(1-41)$, $^qR_0(0-19)$, $^qP_1(2-36)$, $^qR_1(1-24)$, $^qP_2(3-29)$, $^qR_2(3-16)$. One forbidden line is identified as $^rR_0(0)$ $F_2 \leftarrow F_1$ and occasionally single Q branch lines are resolved, for example, the $^rQ_0(1)$ $F_2$ line (Figure 3). The molecular constants of the ground and $\nu_3$ vibrational states of HOH$^+$—Ar obtained from a least-squares fit of the positions of the identified P and R branch lines to Hamiltonian $(1-3)$ are summarized in Table 1. The standard deviation of the fit, $\sigma = 0.015$ cm$^{-1}$, is consistent with the observed line width (0.02 cm$^{-1}$) and the accuracy of the calibration (0.02 cm$^{-1}$). The constants in Table 1 reproduce all line positions to within 0.04 cm$^{-1}$. Experimental and fitted line positions are available upon request.

Figures 3 and 4 show the observed spectra of the $K_a = 1 \leftarrow 0$ and $K_a = 2 \leftarrow 1$ subbands, along with assignments of identified transitions and simulations using the constants in Table 1 and intensities appropriate for a symmetric top molecule.[56] For the simulation of the $K_a = 1 \leftarrow 0$ band, a bimodal Boltzmann distribution using $T_1 = 6.8$ and $T_2 = 18.3$ K with equal weights is used. Such a population distribution is obtained from a Boltzmann plot of the $^rR_0$ line intensities (Figure 5). For the simulation of the $K_a = 2 \leftarrow 1$ subband, $T_1 = 30$ K and $T_2 = 90$ K are used with equal weights. In agreement with previous observations for cluster ions produced in the ion source used, levels with higher rotational quantum numbers have populations corresponding to higher effective temperatures.[23,58] The vibrational temperature derived from the $\nu_1 + \nu_s \leftarrow \nu_s$ sequence bands of $H_2O^+$—Ar and DOH$^+$—Ar, $T_{vib} = 150 \pm 50$ K is even higher. The spectra in Figures 3 and 4 illustrate that, as expected, the spin-rotation splittings decrease with increasing $N$, whereas the asymmetry splittings in subbands involving $K_a$
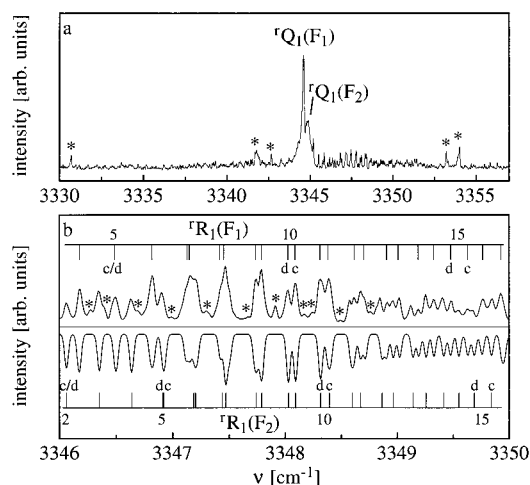
**Figure 4.** (a) Experimental $K_a = 2 \leftarrow 1$ subband of the $\nu_3$ transition of HOH$^+$−Ar. Asterisks indicate identified Q branch heads of the $\nu_3$ band of NH$_4^+$−Ar. (b) Comparison of experimental (top) and simulated (bottom) part of the R branch of the $K_a = 2 \leftarrow 1$ subband with assignments. The asymmetry splitting (c/d) increases with $N$, whereas the spin-rotation splitting ($F_1/F_2$) decreases. Asterisks mark unidentified rotational lines. The simulation is based on the rotational constants in Table 1, a bimodal Boltzmann distribution with $T = 30$ and 90 K with equal weight, and a convolution width of 0.04 cm$^{-1}$.
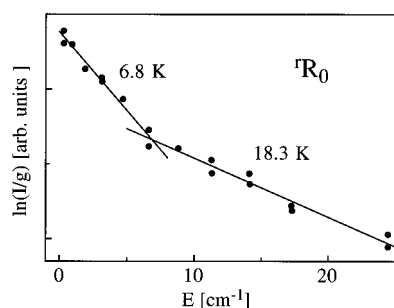


**Figure 5.** Boltzmann plot of the $F_1$ and $F_2$ components of the $K_a = 1 \leftarrow 0$ R branch lines of the $\nu_3$ transition of HOH$^+$−Ar. The intensities, $I$, are approximated by the symmetric top formulas. The parameter $g$ accounts for the Hönl−London and degeneracy factors. The population of energy levels with $N \leq 7$ is best represented by $T_1 = 6.8$ K, whereas for the higher levels $T_2 = 18.3$ K is obtained in a least-squares fit.

$= 1$ increase with $N$. The width of single rotational lines in individual scans is limited by the laser bandwidth (0.02 cm$^{-1}$) and independent of $J$, $N$, and $K_a$, providing a lower limit to the lifetime of the $\nu_3$ state, $\tau_3 > 250$ ps.

Several smaller Q branches are observed at 3330.70, 3341.68, 3341.93, 3342.67, 3353.20, 3354.00 cm$^{-1}$ (indicated by asterisks in Figure 4a). They can be assigned to the various internal rotation subbands of the $\nu_3$ fundamental of the NH$_4^+$−Ar dimer investigated previously.[17,19,20] The NH$_4^+$ ion is produced in the electron impact source from H$_2$O and impurities of N$_2$. Because H$_2$O$^+$ has the same mass as NH$_4^+$, the absorptions of NH$_4^+$−Ar occur in the photodissociation spectrum of H$_2$O$^+$−Ar owing to identical masses of both parent and daughter ions (within the mass resolution of the QMSs employed). Several weaker P/R branch series occurring in the vicinity of the $\nu_3$ fundamental of H$_2$O$^+$−Ar (see for example the weak series marked by asterisks in the top panel of Figure 4b) cannot be attributed to NH$_4^+$−Ar. They probably arise from sequence hot bands of H$_2$O$^+$−Ar of the type $\nu_3 + \nu_x \leftarrow \nu_x$, where $\nu_x$ are intermolecular modes.

The coarse rotational structure of the $\nu_3$ band of HOD$^+$−Ar is similar to the rotational structure of HOH$^+$−Ar (Figure 2).

The Q branches of the perpendicular component have similar spacings in both spectra, confirming that the bound proton is replaced by deuterium leaving the $A$ rotational constant almost unaffected. The spectrum of HOD$^+$−Ar displays a lower signal−to−noise ratio than HOH$^+$−Ar, as for statistical reasons the parent ion intensity is reduced by a factor of 4: HOH$^+$−Ar, HOD$^+$−Ar, DOH$^+$−Ar, and DOD$^+$−Ar occur roughly with the same abundance as they have similar binding energies,[12] and a 1:1 mixture of H$_2$O and D$_2$O is used to prepare HOD$^+$−Ar (complete H/D scrambling is assumed). Consequently, single P and R branch lines could not be identified for HOD$^+$−Ar preventing a detailed rotational analysis. Only the approximate positions of the six observed Q branch maxima originating from $K_a \leq 3$ are reported here (FWHM = 0.6−0.8 cm$^{-1}$): $^rQ_0 = 3307.4$ cm$^{-1}$, $^rQ_1 = 3347.3$ cm$^{-1}$, $^rQ_2 = 3384.8$ cm$^{-1}$, $^pQ_1 = 3264.6$ cm$^{-1}$, $^pQ_2 = 3221.5$ cm$^{-1}$, and $^pQ_3 = 3177.5$ cm$^{-1}$. The estimated band origin, $\nu_0 = 3286.5 \pm 0.5$ cm$^{-1}$, is blue-shifted by $\sim 2.5$ cm$^{-1}$ compared to the corresponding HOH$^+$−Ar transition. Similar to the H$_2$O$^+$−Ar spectrum, the HOD$^+$−Ar spectrum features absorptions attributed to Q branches of the $\nu_3$ band of NH$_3$D$^+$−Ar (at 3303.2, 3314.9, 3326.6, 3337.9, 3349.1 cm$^{-1}$).

*3. Discussion.* Both the vibrational and rotational analyses of the mid-IR spectrum of H$_2$O$^+$−Ar clearly show that the most stable isomer of this dimer has a H-bound HOH$^+$−Ar structure, in agreement with the ab initio calculations.[12] Only this geometry is compatible with the large observed red shift in the $\nu_1$ mode and its large intensity enhancement compared with the $\nu_3$ mode. Moreover, the observed $A$ constant of the complex, $A \sim 22$ cm$^{-1}$, is consistent only with geometries in which one H atom of H$_2$O$^+$ lies on the axis of the two heavy atoms. Furthermore, $C_{2v}$ symmetric structures with two equivalent H atoms (like the bridged or oxygen-bound geometries in Figure 1 of article I) would lead to 1:3 intensity alternations in the spectrum for levels with $A$ and $B$ symmetry (corresponding to their nuclear spin statistical weights), in disagreement with the observations. For similar reasons, the p-bound structure with $C_s$ symmetry can be excluded. The inertial defect, $\Delta_0 = 0.112(8)$ uÅ$^2$, is close to zero confirming the near-planarity of the complex. It is approximately two times larger than the value for H$_2$O$^+$, $\Delta_0 = 0.053$ uÅ$^2$,[39] and most of the difference arises from the large zero-point amplitude of the intermolecular out-of-plane bending motion of the complex. The related neutral OC−HOH complex, which also has a planar H-bonded equilibrium structure with rotational constants and asymmetry ($A = 19.83$, $B = 0.09214$, $C = 0.09127$, $B − C = 0.00087$ cm$^{-1}$) similar to HOH$^+$−Ar, has a much larger inertial defect, $\Delta_0 \sim 0.9$ uÅ$^2$, because of larger out-of-plane zero-point motions in this relatively weakly bound complex.[59]

The rotational constants of HOH$^+$−Ar in Table 1 are used to estimate the geometrical parameters of the intermolecular bond in the ground vibrational state assuming a rigid geometry. (See Figure 1 of article I for the designation of bond lengths and angles.) For this purpose, the H$_2$O$^+$ geometry in the complex is approximated by the experimental H$_2$O$^+$ monomer geometry ($r_0 = 0.999 \pm 0.015$ Å, $\theta_0 = 110.5 \pm 2.5°$)[22,34,37,39] modified by the complexation-induced changes predicted by the ab initio calculations ($\Delta r_{ae} = -0.004$ Å, $\Delta r_{be} = 0.029$ Å, $\Delta\theta_e = 0.4°$).[12] The parameters $R_0 = 1.929(15)$ Å and $\varphi_0 = 175(4)°$ reproduce under these conditions the experimental rotational constants to within 2% (including the quoted errors in the experimental H$_2$O$^+$ structure). They are also compatible with the ab initio values, $R_e = 1.9154$ Å and $\varphi_e = 176.1°$.[12]

**TABLE 1: Experimental Molecular Constants (in cm$^{-1}$) of the Ground and $\nu_3$ Vibrational States of HOH$^+$−Ar Compared with Calculated Equilibrium Values$^a$**

| constant | ground state | $\nu_3$ state | calculated$^b$ |
|---|---|---|---|
| $\nu_0$ | 0.0 | 3283.9062(17)$^c$ | |
| $A$ | 21.9795(22) | 20.9803(22) | 21.4650 |
| $\bar{B}$ | 0.156991(48) | 0.156309(50) | 0.158476 |
| $(B-C) \times 10^3$ | 1.285(16) | 1.348(18) | 1.1700 |
| $B^d$ | 0.157634(49) | 0.156983(51) | 0.159061 |
| $C^d$ | 0.156349(49) | 0.155635(51) | 0.157891 |
| $D_N \times 10^7$ | 2.96(62) | 2.88(68) | |
| $D_{NK} \times 10^5$ | 0.40(31) | 2.54(31) | |
| $D_K \times 10^2$ | 4.855(47) | 3.622(47) | |
| $a$ | 0.21717(100) | 0.20391(93) | |
| $a_0$ | 0.2195(16) | 0.2068(15) | |
| $\epsilon_{aa}$ | −0.6539(26) | −0.6146(24) | |
| $(\epsilon_{bb} + \epsilon_{cc}) \times 10^3$ | −4.6(38) | −5.8(35) | |
| $\Delta$ [u$\text{Å}^2$] | 0.1120(79) | 0.1266(82) | |

$^a$ Standard deviations are given in parentheses. $^b$ Equilibrium constants calculated at MP2/aug-cc-pVTZ MP2 level of theory (ref 12). $^c$ Absolute accuracy is 0.02 cm$^{-1}$. $^d$ Derived from $\bar{B}$ and $B-C$.

The dissociation energy of the complex is calculated as $D_0 \sim 2200$ cm$^{-1}$.[12] The modest blue shift of the $\nu_3$ vibration upon complexation, $\Delta\nu_3 = 24.9$ cm$^{-1}$, reflects the relatively small decrease in the intermolecular binding energy upon $\nu_3$ excitation ($\sim 1\%$). It is therefore justified to assume that the large decrease in the rotational $A$ constant upon $\nu_3$ excitation of 5% ($B$ and $C$ decrease by $<0.5\%$) mainly arises from an effective stretching of the free O—H bond associated with excitation of one quantum of this mode. From the change in the rotational constants, the increase in the effective free O—H separation upon $\nu_3$ excitation can be estimated as $0.022 \pm 0.003$ Å. A very similar increase in the interatomic distance is observed for $\nu_1$ excitation in OH$^+$ (0.024 Å).[60] The increase in the inertial defect of 13% upon $\nu_3$ excitation of H$_2$O$^+$−Ar is contrasted with a decrease of 11% in the monomer,[37] presumably because of the large change in the normal modes upon Ar complexation.

In contrast to $\nu_3$, excitation of $\nu_1$ has a great effect on the intermolecular interaction. The observed red shift, $\Delta\nu_1 = -541$ cm$^{-1}$, implies that the dissociation energy of the complex increases by as much as 20%. This is consistent with the observed increase of the intermolecular stretching force constant from 29 to 39 N/m. The $\nu_1$ mode is mainly a stretching motion of the O—H donor bond, and vibrational excitation leads to an enhanced proton shift toward the Ar atom, with the effect of stabilizing and shortening the intermolecular bond. This effect is typical for neutral and ionic hydrogen bonds and its magnitude is related to the interaction strength.[10,26,61,62] The intermolecular bond contraction is indicated by the heads in the P branches of the overlapping $\Delta K_a = 0$ subbands of the $\nu_1$ fundamental. Figure 6 shows the experimental contour of the $\nu_1$ band together with a simulation using the molecular constants of Table 1 for the ground state, a convolution width of 0.2 cm$^{-1}$ and Boltzmann distributions with temperatures of 20 K for $K_a = 0\leftarrow 0$, 90 K for $K_a = 2\leftarrow 2$, and 20 and 90 K (with 9:1 weight) for $K_a = 1\leftarrow 1$. The $\nu_1$ state constants are approximated by the ground-state parameters, except $\nu_0 = 2672.22$ cm$^{-1}$, $\bar{B}' = 0.1615$ cm$^{-1}$, and $A' = 21.64$ cm$^{-1}$, which are adjusted to reproduce the observed band profile ($A'$, $D_K'$, and $\nu_0$ are highly correlated). The change in the $\bar{B}$ constant (which could reliably be estimated from the Q and P branch heads of the $K_a = 1\leftarrow 1$ subband) corresponds to an intermolecular bond contraction of the order of 0.05 Å upon $\nu_1$ excitation, a value typical for related AH$^+$−Ar complexes.[13,15,24] The intermolecular stretching frequency in the $\nu_1$ state (232 cm$^{-1}$) is 16% higher than the corresponding
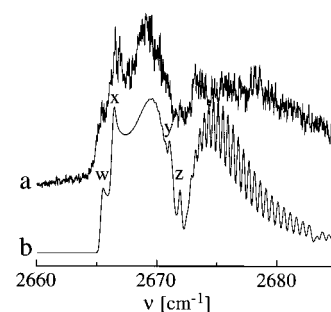


**Figure 6.** Experimental (a) and simulated IR spectrum (b) of the $\nu_1$ band of HOH$^+$−Ar. The $^qQ_2$ ($y$) and $^qQ_1$ ($z$) branches and the heads of the $^qP_2$ ($w$) and $^qP_1$ ($x$) branches are indicated. The additional signal in the blue wing of the experimental transition arises from sequence hot bands, which are not included in the simulation.

value for the ground state ($\nu_s = 200$ cm$^{-1}$). This observation is consistent with the increase in the intermolecular interaction upon $\nu_1$ excitation. The band contour of the parallel $\nu_1 + \nu_s$ transition is almost unshaded, as the effective bond lengthening upon $\nu_s$ excitation approximately compensates for the bond contraction caused by $\nu_1$ excitation.

According to the simulations, the rotational line width in the experimental $\nu_1$ spectrum has to be $>0.4$ cm$^{-1}$ to completely wash out the rotational fine structure (Figure 6), but $<0.8$ cm$^{-1}$ to still display the observed coarse structure. It is assumed that the homogeneous broadening arises from fast relaxation processes in the $\nu_1$ state, that is, intracomplex vibrational energy redistribution and/or vibrational predissociation. From the upper and lower limits for the line width, the lifetime of the $\nu_1$ state can be bracketed as $\tau_1 = 10 \pm 5$ ps. In contrast, the lifetime of the higher-lying $\nu_3$ state is much longer ($\tau_3 > 250$ ps), implying that the relaxation dynamics are highly mode selective and cannot be rationalized by statistical theories. In general, the coupling strength between intramolecular and intermolecular degrees of freedom is correlated with the complexation-induced frequency shift of the excited intramolecular state: the larger the shift, the stronger the coupling, and the shorter the lifetime.[10,24,63−66] For example, in H-bound AH$_k^+$−B dimers involving ions with more than 1 equivalent proton (e.g., HNH$^+$−Ar or H$_3$O$^+$−H$_2$)[24,65] the bound A—H stretch states always have significantly shorter lifetimes and larger frequency shifts than the free A—H stretch states. The values for HOH$^+$−Ar ($\tau_1 \sim 10$ ps, $\tau_3 > 250$ ps, $\Delta\nu_1 = -541$ cm$^{-1}$ and $\Delta\nu_3 = 25$ cm$^{-1}$) are qualitatively similar to those of the related HNH$^+$−Ar complex ($\tau_1 \sim 25$ ps, $\tau_3 > 130$ ps, $\Delta\nu_1 = -300 \pm 50$ cm$^{-1}$, and $\Delta\nu_3 = -73.6$ cm$^{-1}$).[24] The HOH$^+$−Ar dimer has a larger binding energy ($D_e = 2484$ cm$^{-1}$) compared to HNH$^+$−Ar ($D_e \sim 1750$ cm$^{-1}$), which accounts for the stronger coupling, the larger $\nu_1$ red shift, and the shorter $\nu_1$ lifetime.

The rotational structure of the $\nu_3$ band of H$_2$O$^+$−Ar allows for the determination of the spin−rotation constants in both the ground and $\nu_3$ vibrational states. The derived spin-rotation constants $a$ and $a_0$ are listed in Table 1. (The spin-rotation parameter $b$ is set to zero, as H$_2$O$^+$−Ar is very close to a symmetric top.) The $a$, $a_0$, and $b$ constants are related to another equivalent set of constants, namely $\epsilon_{aa}$, $\epsilon_{bb}$, and $\epsilon_{cc}$,[57] which are more convenient for comparison with the corresponding constants of H$_2$O$^+$.[39] In the present case, only $\epsilon_{aa}$ and $\epsilon_{bb} + \epsilon_{cc}$ can be determined for each vibrational state (Table 1). Assuming that the electromagnetic properties of the $^2B_1$ electronic ground state of H$_2$O$^+$ are not affected by the weak interaction with Ar, the $\epsilon_{ii}$ parameters of H$_2$O$^+$ and H$_2$O$^+$−Ar are related to each other by scaling them with the ratios of the respective moments

**TABLE 2: Comparison of Several Properties of Proton-bound AH$^+$−Ar Dimers**

| AH$^+$−Ar | SiOH$^+$−Ar[a] | OCH$^+$−Ar[b] | HNH$^+$−Ar[c] | HOH$^+$−Ar | OCOH$^+$−Ar[d] | NNH$^+$−Ar[e] |
|---|---|---|---|---|---|---|
| $\Delta PA_{A-Ar}$ [kJ/mol][f] | 410 | 225 | 221 | 224 | 171 | 125 |
| $D_e$ [cm$^{-1}$] | 1117 | 1541 | 1773 | 2484 | 2379 | 2881 |
| $\Delta\nu_1$ [cm$^{-1}$] | −217 | −274 | −300 ± 50 | −541 | −704 | −728 |
| $k_s$ [N/m] | 13 | 17 | 20 | 29 | | 38 |
| $R_{H-Ar}$ [Å] | 2.19 | 2.13 | 2.06 | 1.93 | | 1.90 |

[a] Ref 15. [b] Refs 13 and 14. [c] Ref 24. [d] Ref 26. [e] Refs 10, 82, and 83. [f] Refs 80 and 81.

of inertia. Moreover, the rotation of the inertial axis system upon complexation by an angle α around the c-axis has to be taken into account. From the structures derived from the analysis of the rotational constants, a value of α = 34° is obtained for the ground vibrational state. This value differs somewhat from that estimated from the spin-rotation constants, α = 26 ± 1°. The difference may arise from small changes in the electronic wave function of H$_2$O$^+$ upon Ar complexation and/or the neglect of nonrigidity arising from large amplitude motions in the dimer. Excitation of $\nu_3$ leads to a 5% decrease in the A constant of H$_2$O$^+$−Ar, compatible with the 6% reduction in $\epsilon_{aa}$.

The preliminary analysis of IR spectra of H$_2$O$^+$−He and H$_2$O$^+$−Ne reveals splittings that are attributed to hindered internal rotation of H$_2$O$^+$.[67] To estimate the magnitude of the tunneling splittings in H$_2$O$^+$−Ar, two tunneling paths for proton exchange are considered: internal rotation of H$_2$O$^+$ around its b- and c-axes, respectively. Both tunneling motions are approximated by one-dimensional potential expansions of the form

$$V(\phi) = \sum_n \frac{V_n}{2}(1 - \cos(n\phi)) \qquad (4)$$

The one-dimensional Schrödinger equation is solved using the B and C rotational constants of H$_2$O$^+$ as internal rotor constants, respectively ($B_0 = 12.42$ cm$^{-1}$, $C_0 = 8.47$ cm$^{-1}$).[36] The potential for the in-plane rotation (i.e., rotation around the c-axis) is obtained by fitting the coefficients $V_n$ to the points of the rigid monomer PES along the minimum energy path calculated at the MP2/aug-cc-pVTZ$^\#$ level[12]: $V_n = -1742.2$, −745.0, 748.2, and −224.3 cm$^{-1}$ for n = 1−4. The tunneling splitting obtained for this potential is of the order of 0.002 cm$^{-1}$ for the ground vibrational state. The potential for rotation around the b (=C$_2$) axis of H$_2$O$^+$ is approximated by a 2-fold barrier; the $V_2$ parameter is estimated to be larger than 550 cm$^{-1}$, which corresponds to the difference between the energies of the H-bound and p-bound minima calculated at the MP2/aug-cc-pVTZ$^\#$ level.[12] An upper limit for the tunneling splitting arising from this motion is derived as 0.003 cm$^{-1}$ for the ground vibrational state. Based on these simple one-dimensional model calculations, the expected tunneling splittings arising from proton exchange are well below the experimental resolution. A similar situation was recently observed for the related HClH$^+$−Ar and HNH$^+$−Ar complexes.[24,27] Tunneling splittings of the order of 1−2 cm$^{-1}$ are observed in the spectra of H$_3$$^+$−Ar and NH$_4$$^+$−Ar,[19,68] and these have been rationalized by the larger ratios of the effective internal rotor constant and the barriers for hindered internal rotation.[27] It appears that in H-bound AH$_2$$^+$−Ar dimers the probability for proton exchange is smaller than for related AH$_k$$^+$−Ar dimers with k = 3,4. This observation follows the rough rule of thumb for AH$_k$$^+$−Ar dimers: the more H atoms in the AH$_k$$^+$ ion, the shorter the tunneling path between equivalent minima and the smaller the barriers for internal rotation, giving rise to higher tunneling probabilities between these minima.[10,19]

Table 2 compares several properties of H$_2$O$^+$−Ar with those of related H-bound AH$^+$−Ar dimers studied by the same experimental and theoretical methods. The listed binding energies are calculated at the MP2/aug-cc-pVTZ$^\#$ level, whereas the $\nu_1$ red shifts ($\nu_1 = \nu_{A-H}$ stretch), the intermolecular separations ($R_{H-Ar}$), and the intermolecular stretching force constants ($k_s$) are experimental values. All considered AH$^+$−Ar complexes feature (near) linear H-bonds and the relative strengths of the A−H and H−Ar bonds are related to the difference in the proton affinities (PA) of the two bases, $\Delta PA_{A-Ar} = PA_A - PA_{Ar}$.[10,15,69] As PA$_A$ ≫ PA$_{Ar}$ for all considered bases (A = SiO, CO, NH, OH, CO$_2$, and N$_2$), the AH$^+$−Ar dimers are composed of an AH$^+$ ion, which is more or less perturbed by the Ar ligand. The perturbation results in a flattening of the potential for the proton motion, which is reflected in the red shift of the A−H stretch vibration, $\Delta\nu_1$. In general, the smaller $\Delta PA_{A-Ar}$, the stronger and shorter the intermolecular bond (i.e., $D_e$ and $k_s$ increase, whereas $R_{H-Ar}$ decreases) and the larger the perturbation of AH$^+$ upon Ar complexation (i.e., the magnitude of $\Delta\nu_1$ increases). The intermolecular bond in H$_2$O$^+$−Ar appears to be somewhat stronger than expected from the PA of OH, and this effect may be attributed to the radical character of H$_2$O$^+$ in its $^2B_1$ electronic ground state (see article I).[12]

Comparison of the properties of H$_2$O$^+$−Ar with those of the corresponding neutral dimer reveals that ionization greatly influences the PES. The PES of H$_2$O−Ar derived from microwave and IR data (AW2 potential) features also a planar global minimum with a translinear H-bond.[70] However, in contrast to H$_2$O$^+$−Ar,[12] the bond is much weaker ($D_e \sim 140$ vs 2484 cm$^{-1}$) and the barriers to internal rotation are much smaller ($V_b < 60$ vs $V_b > 500$ cm$^{-1}$). The latter are comparable to the H$_2$O rotational constants leading to only slightly hindered internal rotation. In general, the presence of the charge causes the cationic complex to be more rigid with a much stronger and more directional intermolecular bond. This effect is, for example, visible in the significantly different intermolecular stretch frequencies ($\nu_s \sim 30$ vs 200 cm$^{-1}$ for H$_2$O−Ar vs H$_2$O$^+$−Ar). Moreover, the effects of Ar complexation on H$_2$O are very small and, as a result of the weak coupling, the predissociation lifetimes are long and the complexation-induced frequency shifts are small (< few cm$^{-1}$).[71,72]

**B. H$_2$O$^+$−Ar$_2$ Trimer (n = 2).** According to the IR spectrum and the calculated PES of H$_2$O$^+$−Ar,[12] the H-bound configuration corresponds to the most stable dimer structure, whereas other binding sites (e.g., the p-bound structure) are less stable. Consequently, the most stable H$_2$O$^+$−Ar$_2$ trimer geometry is expected to have two H-bonds leading to a planar Ar−HOH$^+$−Ar structure with C$_{2v}$ symmetry (Figure 1f, article I). Indeed, the IR spectrum of H$_2$O$^+$−Ar$_2$ (Figures 7 and 8, Table 3) is consistent with such a trimer structure. Similar to H$_2$O$^+$, both O−H bonds are equivalent in Ar−HOH$^+$−Ar and the O-H stretch normal modes are symmetric and antisymmetric combinations of the two O−H local oscillators, $\nu_1$ and $\nu_3$. Com-
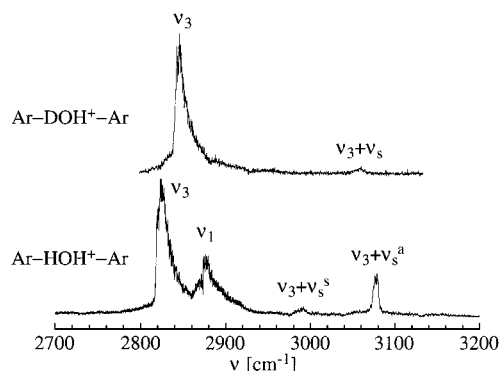
**Figure 7.** Mid-IR photodissociation spectra of H$_2$O$^+$−Ar$_2$ (bottom) and HDO$^+$−Ar$_2$ (top) with assignments.
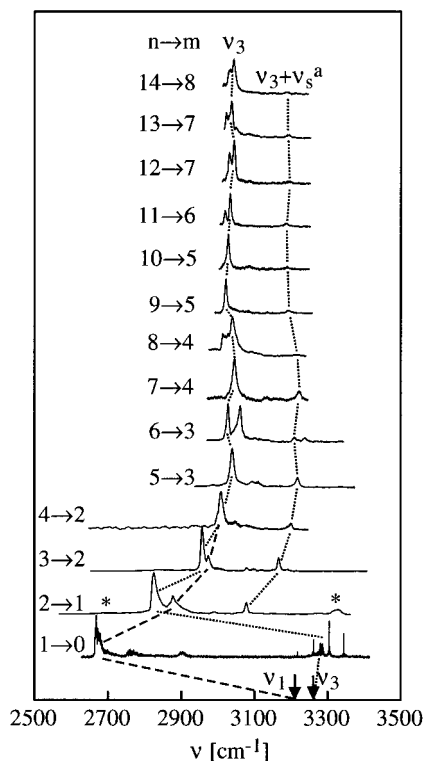


**Figure 8.** Mid-IR photodissociation spectra of H$_2$O$^+$−Ar$_n$ recorded in the dominant H$_2$O$^+$−Ar$_m$ fragment channel (indicated as $n \rightarrow m$). As the spectra are composed of several scans, the relative intensities of widely separated bands are not reliable. In particular, the spectra of $n = 1-4$ are recorded with two different mirror sets ($\leq$ and $\geq 3000$ cm$^{-1}$), while the spectra of $n > 4$ could be recorded with one set. The connecting lines indicate the bands assigned to $\nu_1$, $\nu_3$, and $\nu_3 + \nu_s^a$ of the most abundant isomer of each cluster size. The arrows show the position of the $\nu_1$ and $\nu_3$ band origins of bare H$_2$O$^+$. Absorptions assigned to a less stable isomer of $n = 2$ (denoted II) are indicated by asterisks.

plexation with Ar weakens the O−H bonds, leading to substantial red shifts of both vibrations with respect to H$_2$O$^+$ (Figure 8). The $\nu_1$ and $\nu_3$ fundamentals of Ar−HOH$^+$−Ar occur as strong transitions at 2875 and 2821 cm$^{-1}$ (Figure 7) and the derived red shifts of −337 and −438 cm$^{-1}$ are in good agreement with the calculated values (−303 and −410 cm$^{-1}$).[12] The $\nu_3$ band is more intense than $\nu_1$ and the order of both modes inverts upon complexation with two Ar atoms, again in agreement with the theoretical predictions. The assignments of $\nu_1$ and $\nu_3$ are also supported by the observed band profiles: $\nu_1$ is a broader perpendicular band with unresolved $\Delta K_a = \pm 1$ subbands, whereas $\nu_3$ is a narrower parallel band composed of

**TABLE 3: Band Maxima and Widths (Full Width Half-Maximum) of Vibrational Transitions Observed in the IR Photodissociation Spectra of H$_2$O$^+$−Ar$_n$ with Assignments**

| $n$ | position (fwhm) | assignments[a] | $n$ | position (fwhm) | assignments[a] |
|---|---|---|---|---|---|
| 1 | 2672.22[b] | $\nu_1$ | 7 | 3045 (15) | $\nu_3$ |
| | 2705 (20) | $\nu_1 + \nu_s - \nu_s$ | | 3220 (10) | $\nu_3 + \nu_s^a$ |
| | 2767 (25) | $2\nu_2$ | | | |
| | 2904.5 (15) | $\nu_1 + \nu_s$ | 8 | 3014 (8) | $\nu_3$ (II) |
| | 3283.91[b] | $\nu_3$ | | 3029 (8) | $\nu_3$ (III) |
| | | | | 3038 (14) | $\nu_3$ |
| 2 | 2700 (50) | $\nu_1$ (II) | | 3185 (11) | $\nu_3 + \nu_s^a$ (II) |
| | 2821 (10) | $\nu_3$ | | 3201 (6) | $\nu_3 + \nu_s^a$ (III) |
| | 2875 (13) | $\nu_1$ | | 3213 (9) | $\nu_3 + \nu_s^a$ |
| | 2990 (9) | $\nu_3 + \nu_s^s (a_1)$ | | | |
| | 3077 (8) | $\nu_3 + \nu_s^a (b_2)$ | 9 | 3022 (6) | $\nu_3$ |
| | 3324 (30) | $\nu_3$ (II) | | 3195 (11) | $\nu_3 + \nu_s^a$ |
| 3 | 2956 (9) | $\nu_3$ | 10 | 3027 (6) | $\nu_3$ |
| | 2973 (8) | $\nu_1$ | | 3188 (16) | $\nu_3 + \nu_s^a$ |
| | 3078 (8) | $\nu_3 + \nu_s^s$ | | | |
| | 3098 (8) | $\nu_1 + \nu_s^s$ | 11 | 3018 (6) | $\nu_3$ (II) |
| | 3120 (10) | | | 3033 (7) | $\nu_3$ |
| | 3166 (7) | $\nu_3 + \nu_s^a$ | | 3173 (8) | $\nu_3 + \nu_s^a$ (II) |
| | 3190 (10) | $\nu_1 + \nu_s^a$ | | 3184 (10) | $\nu_3 + \nu_s^a$ |
| 4 | 3008 (15) | $\nu_3/\nu_1$ | 12 | 3026 (8) | $\nu_3$ (II) |
| | 3199 (9) | $\nu_3 + \nu_s^a$ | | 3039 (8) | $\nu_3$ |
| | | | | 3184 (16) | $\nu_3 + \nu_s^a$ |
| 5 | 3038 (9) | $\nu_3$ | | | |
| | 3216 (10) | $\nu_3 + \nu_s^a$ | 13 | 3024 (7) | $\nu_3$ (II) |
| | | | | 3037 (10) | $\nu_3$ |
| 6 | 3027 (6) | $\nu_3$ | | 3185 (10) | $\nu_3 + \nu_s^a$ |
| | 3059 (8) | $\nu_3$ (II) | | | |
| | 3208 (13) | $\nu_3 + \nu_s^a$ | 14 | 3033 (8) | $\nu_3$ (II) |
| | 3234 (10) | $\nu_3 + \nu_s^a$ (II) | | 3042 (8) | $\nu_3$ |
| | | | | 3183 (6) | $\nu_3 + \nu_s^a$ (II) |
| | | | | 3191 (10) | $\nu_3 + \nu_s^a$ |

[a] II and III are attributed to less stable isomers. [b] Band origins.

overlapping $\Delta K_a = 0$ subbands. The $\nu_1$ and $\nu_3$ modes in Ar−HOD$^+$−Ar are localized O−D and O−H stretch oscillators and the spectrum features thus only one transition in the 2800−2900 cm$^{-1}$ range, corresponding to the O−H stretch ($\nu_3$, Figure 7). In agreement with the theoretical prediction, the measured frequency of 2844 cm$^{-1}$ lies roughly midway between the $\nu_1$ and $\nu_3$ modes of Ar−HOH$^+$−Ar.[12] The O−D stretch of Ar−HOD$^+$−Ar (calculated as ~2040 cm$^{-1}$) is shifted out of the investigated spectral range.[12]

The Ar−HOH$^+$−Ar spectrum shows two further transitions at 2990 and 3077 cm$^{-1}$. Inspection of the spectra of larger clusters (Figure 8) shows that these bands shift together with the $\nu_3$ (and $\nu_1$) bands as the cluster size increases. They must therefore be attributed to combination bands of $\nu_3$ (or $\nu_1$) with intermolecular modes. Ab initio calculations predict for the trimer only two intermolecular modes in the frequency range 50−300 cm$^{-1}$, namely the symmetric and antisymmetric linear combinations of the intermolecular H−Ar stretching modes, $\nu_s^s(a_1) = 166$ cm$^{-1}$ and $\nu_s^a(b_2) = 208$ cm$^{-1}$.[12] The most probable assignment of the two observed bands at 2990 and 3077 cm$^{-1}$ is thus $\nu_3 + \nu_s^s$ and $\nu_3 + \nu_s^a$, yielding $\nu_s^s = 169$ cm$^{-1}$ and $\nu_s^a = 256$ cm$^{-1}$ in the $\nu_3$ state. The average value of the two $\nu_s$ frequencies is 213 cm$^{-1}$, about 20 cm$^{-1}$ lower than the dimer $\nu_s$ value in the $\nu_1$ state (232 cm$^{-1}$). Apparently, the formation of the second intermolecular H−Ar bond weakens the first one. Ab initio calculations predict $D_0 = 2200$ and 1800 cm$^{-1}$ for the binding energies of the first and second Ar ligand, respectively.[12] This large and noncooperative three-body effect

is also indicated by the average value of $\nu_1$ and $\nu_3$ in the Ar—HOH$^+$—Ar trimer (2848 cm$^{-1}$) which is substantially higher than the bound O—H stretch of the dimer ($\nu_1 = 2672$ cm$^{-1}$), implying that the proton donor O—H bonds in the trimer are stronger than that of the dimer. The Ar—HOD$^+$—Ar spectrum features a weak transition at 3059 cm$^{-1}$, which is separated by 215 cm$^{-1}$ from the corresponding O—H stretch transition, $\nu_3$. This value is close to the average value of the $\nu_s^s$ and $\nu_s^a$ frequencies of Ar—HOH$^+$—Ar in the $\nu_3$ state (213 cm$^{-1}$). Such a $\nu_s$ value is expected if the two intermolecular H—Ar stretches decouple upon single deuteration. Indeed, the $\nu_3$ mode in Ar—HOD$^+$—Ar is a localized O—H stretch, which via efficient coupling selectively strengthens the intermolecular H—Ar bond but not the D—Ar bond. Thus, the two intermolecular H—Ar and D—Ar oscillators are decoupled in the $\nu_3$ state of HDO$^+$—Ar$_2$ (owing to different force constants), and the observed band at 3059 cm$^{-1}$ is hence attributed to $\nu_3 + \nu_s$, where $\nu_s$ is the localized H—Ar stretch.

The Ar—HOH$^+$—Ar spectrum displays two weak and broad transitions at $3324 \pm 15$ and $2700 \pm 25$ cm$^{-1}$ (indicated by asterisks in Figure 8), that is, in the range of the free and bound O—H stretch vibrations of the H-bound dimer. These absorptions can be assigned tentatively to a less stable isomer of H$_2$O$^+$—Ar$_2$ (denoted isomer II in Table 3) featuring a H-bond and a p-bond. Both binding sites are minima on the MP2 potential of the dimer.[12] Complexation at the p-bound site slightly strengthens the O—H bonds. For example, the calculated blue shifts of the p-bound H$_2$O$^+$—Ar dimer compared with bare H$_2$O$^+$ amount to 48 and 69 cm$^{-1}$ for $\nu_1$ and $\nu_3$, respectively.[12] For H$_2$O$^+$—Ar$_2$ the measured blue shifts for the bound and free O—H stretch fundamentals upon attachment of the second Ar at the p-bound site of the H-bound H$_2$O$^+$—Ar dimer are $28 \pm 25$ and $40 \pm 15$ cm$^{-1}$, respectively. Because the intensities of both O—H stretch transitions of this isomer are much weaker than the corresponding bands of the most stable trimer featuring two H-bonds, its population in the molecular beam must be significantly smaller.

All vibrational transitions of the H$_2$O$^+$—Ar$_2$ complex are only observed in the H$_2$O$^+$—Ar fragment channel. No signal has been detected in the H$_2$O$^+$ channel. This observation implies that the absorbed photon energy (2700–3320 cm$^{-1}$) is not sufficient to evaporate both Ar ligands of either isomer, a conclusion consistent with the calculated binding energies of ~4000 cm$^{-1}$ for the first two Ar ligands in the most stable isomer (two H-bonds) and ~3500 cm$^{-1}$ for isomer II (one H-bond and one p-bond).[12] In addition, it can be concluded that the complexes probed in the octopole are cold and two-photon processes are not observed at the laser intensities used (~0.1 mJ/mm$^2$).

**C. Larger H$_2$O$^+$—Ar$_n$ Clusters ($n = 3-14$).** Figure 8 compares the IR spectra of H$_2$O$^+$—Ar$_n$ for $n = 1-14$. The observed band maxima are summarized in Table 3, along with the suggested assignments. Typical bandwidths of the unresolved transitions range from 5 to 15 cm$^{-1}$. The bands show distinct shifts and splittings as a function of cluster size, which are used to discuss possible cluster structures. The dimer PES features two deep H-bound minima, whereas all other binding sites are considerably less stable. Under the realistic assumption that three-body forces are not very important for the larger clusters, the H$_2$O$^+$—Ar$_n$ structures with $n \geq 3$ will be composed of a relatively stable Ar—HOH$^+$—Ar trimer core (with two strong H—bonds), to which further ligands are weakly attached. This scenario is supported by the spectra of H$_2$O$^+$—Ar$_n$ with $n > 2$, which are similar in appearance to the trimer spectrum. The dominant band in each spectrum is assigned to the $\nu_3$ vibration of H$_2$O$^+$ within the H$_2$O$^+$—Ar$_n$ cluster. Each spectrum features
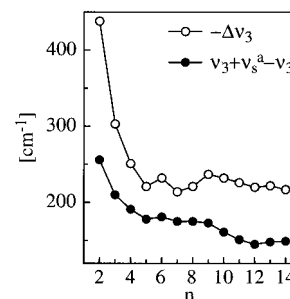


**Figure 9.** Complexation induced red shift of $\nu_3$ ($-\Delta\nu_3$) and intermolecular stretching frequency in the $\nu_3$ state ($\nu_3 + \nu_s^a - \nu_3$) of the most stable isomers of H$_2$O$^+$—Ar$_n$ ($n = 2-14$).
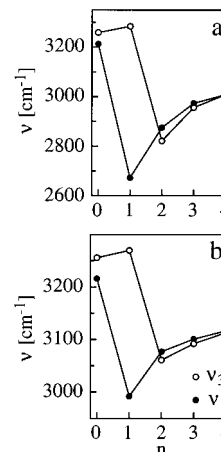


**Figure 10.** Comparison of experimental (a, Table 3) and calculated (b, Table 11 in article I) $\nu_1$ and $\nu_3$ frequencies of H$_2$O$^+$—Ar$_n$ ($n = 0-4$).

a weaker satellite band located 150–200 cm$^{-1}$ to the blue of $\nu_3$, which shifts in the same way as $\nu_3$ as the cluster size increases. It is assigned to a combination band of $\nu_3$ with the antisymmetric combination of the two intermolecular H—Ar stretch oscillators (denoted $\nu_s^a$) by comparison with the Ar—HOH$^+$—Ar spectrum and the ab initio calculations.[12] Apparently, the $\nu_3$ and $\nu_s^a$ normal modes and their IR intensities in H$_2$O$^+$—Ar$_n$ are not much affected upon complexation of the strongly bound Ar—HOH$^+$—Ar chromophore with further Ar ligands. Figure 9 shows that the red shift of $\nu_3$ and the $\nu_s^a$ frequency in the $\nu_3$ state have very similar cluster-size dependencies. This correlation may be expected, because both modes are coupled through the intermolecular H-bonds: $\nu_3$ is the asymmetric O—H stretch and $\nu_s^a$ the asymmetric H—Ar stretch. The weaker the intermolecular H—Ar interaction (i.e., the lower $\nu_s^a$), the stronger the intramolecular O—H bonds (i.e., the higher $\nu_3$ and the smaller $|\Delta\nu_3|$).

The prominent bands in the IR spectra of H$_2$O$^+$—Ar$_3$ and H$_2$O$^+$—Ar$_4$ are interpreted in terms of cluster geometries where one or two Ar atoms, respectively, are attached to opposite sites of the $2p_y$ orbital of the $C_{2v}$ symmetric Ar—HOH$^+$—Ar trimer core (i.e., structures with $C_s$ and $C_{2v}$ symmetry for $n = 3$ and 4). Both O—H stretch modes, $\nu_1$ and $\nu_3$, feature blue shifts with respect to $n = 2$ (135 and 187 cm$^{-1}$ in $\nu_3$), because of the effect of O—H bond contraction upon Ar complexation at the p-bound site. This effect is caused by partial charge transfer from Ar to the $2p_y$ orbital of O.[12] The observed shifts are nonadditive implying that the p-bonds in the $n = 4$ complex are somewhat weaker than that in the $n = 3$ complex. A similar noncooperative three-body effect for the first two H-bonds has been discussed in section III.B. Figure 10 compares the experimental $\nu_1$ and

$\nu_3$ frequencies for $n = 0-4$ with those calculated at the HF/aug-cc-pVTZ$^\#$ level (Table 11, article I).[12] Although the magnitude of the calculated shifts is smaller than the experimental ones (due to the underestimation of the intermolecular interaction at the HF level), both the relative shifts and the intensity ratios are reproduced qualitatively, facilitating the spectral assignments. The splitting between $\nu_1$ and $\nu_3$ decreases (they overlap for $n = 4$), and the calculated intensity of $\nu_3$ is about four to five times higher than that of $\nu_1$, in qualitative agreement with the observed ratio of ∼2. The measured $\nu_s^a$ frequencies in the $\nu_3$ state are 256, 210, and 191 cm$^{-1}$ for $n = 2-4$ and show the same qualitative trend as the values calculated at the HF level for the ground vibrational state (140, 133, and 127 cm$^{-1}$). Again, the calculated values are lower, because the HF level underestimates the interaction.

There are additional weaker transitions observed in the $n = 3$ spectrum (Figure 8, Table 3). The band at 3078 cm$^{-1}$ may tentatively be assigned to $\nu_3 + \nu_s^s$, where $\nu_s^s$ is the symmetric intermolecular H−Ar stretch. The value of $\nu_s^s$ is lower for $n = 3$ than for $n = 2$ (122 vs 169 cm$^{-1}$) owing to the weaker intermolecular H-bonds in the $n = 3$ complex. Possible assignments for the bands at 3098 and 3190 cm$^{-1}$ are $\nu_1 + \nu_s^s$ and $\nu_1 + \nu_s^a$. In this case, the derived $\nu_s^s$ and $\nu_s^a$ frequencies in the $\nu_1$ state (125 and 217 cm$^{-1}$) would be similar to those of the $\nu_3$ state (122 and 210 cm$^{-1}$). Such a situation is expected, because both the $\nu_1$ and $\nu_3$ frequencies are shifted by a similar amount from the $H_2O^+$ values, indicating that the intermolecular interaction is similar in both intramolecular vibrational states.

Because no calculations are available for the clusters with $n \geq 5$, the interpretation of further cluster growth relies only upon the spectroscopic information and is less certain. According to the ab initio calculations, the $\nu_1$ band is ∼5 times weaker than $\nu_3$ in the monomer, and complexation with two Ar atoms does not drastically change this ratio. Similarly, the $\nu_3$ band of $H_2O^+$ deposited in a neon matrix is significantly stronger than $\nu_1$.[42] As larger $H_2O^+-Ar_n$ clusters are composed of the $n = 2$ core, it is expected that $\nu_3$ will be much more intense than $\nu_1$ also in complexes with n>2. Consequently, the single intense band of the $n = 5$ cluster in the O−H stretch region (at 3038 cm$^{-1}$) is assigned to $\nu_3$ (similar to the $n = 4$ cluster, the weaker $\nu_1$ fundamental may be blended by the stronger $\nu_3$ band). Inspection of Figure 9 reveals that the $n = 5$ complex has a smaller $\nu_3$ red shift than $n = 2-4$, that is, the intermolecular H-bonds are weakened by the attachment of the fifth Ar atom. Moreover, $n = 5$ appears to have a special geometry, because both $\nu_3$ and $\nu_s$ display "singularities" at this cluster size. A possible "magic" structure is one where the fifth Ar atom is attached to a $C_{2v}$ symmetric $H_2O^+-Ar_4$ on the $C_2$ axis, where it can interact with all four other Ar ligands. In this configuration, the fifth Ar atom may weaken the intermolecular bonds to the first two H-bound Ar ligands, explaining the blue shift in $\nu_3$ and the relatively small $\nu_s$ frequency.

From $n = 6$ onward, the changes in $\nu_3$ and $\nu_s^a$ are rather small compared with $n < 6$ (Figures 8 and 9). Apparently, further Ar ligands are attached to binding sites with little influence on both the O−H and H−Ar bonds. The cluster growth probably proceeds by filling the first Ar solvation shell around an interior $H_2O^+$ ion. The alternative formation of clusters where $H_2O^+$ is located on the surface of an $Ar_n$ cluster is less likely, as the dimer MP2 potential features optimal interaction energies of $D_{min} > 350$ cm$^{-1}$ between Ar and $H_2O^+$ for any angular orientation. This is much larger than the Ar−Ar interaction of about 100 cm$^{-1}$.[73] The details of solvation shell filling are not obvious from the spectra in Figure 8.

Moreover, splittings of the $\nu_3$ band (and also $\nu_3 + \nu_s^a$) indicate the presence of more than one isomer for $n = 6, 8$, and $11-14$. These splittings are not attributed to the appearance of $\nu_1$ shifted away from $\nu_3$, because the relative intensity ratios of the various components depend on the expansion conditions. Further support of this interpretation is provided by the spectra of $HDO^+-Ar_n$ ($n = 6$), because one band should be largely red-shifted upon single deuteration if the splitting arises from the $\nu_1/\nu_3$ doublet of a single isomer. However, the occurrence of the $\nu_3$ and $\nu_3 + \nu_s^a$ doublets for $n = 6$ is independent of single deuteration, as expected if they stem from two different isomers. As the band at 3027 cm$^{-1}$ is always more intense than the 3059 cm$^{-1}$ band, it is attributed to $\nu_3$ of the most stable $n = 6$ isomer (Figure 8, Table 3). The data in Figure 9 are plotted only for the most stable isomers of each cluster size. The absorptions of less stable isomers, denoted II and III, are listed in Table 3.

No Ar matrix isolation studies on $H_2O^+$ have been performed, making it impossible at this stage to compare the $H_2O^+-Ar_n$ band shifts with the bulk limit ($n = \infty$). It is also not clear how many Ar ligands are necessary to close the first solvation shell and whether the shifts are converged at the largest cluster size investigated ($n = 14$). The present work is limited to cluster sizes $n \leq 14$ by the mass range of the mass spectrometers and not by signal-to-noise. Large incremental $\nu_3$ shifts are observed up to $n \sim 5$ and subsequent changes are much smaller (Figure 9). For example, the incremental shifts are all >30 cm$^{-1}$ for $n \leq 5$, whereas they are less than 20 cm$^{-1}$ for $n = 6-14$. The $\nu_3$ frequencies of $n = 6-14$ are all within 3034 ± 12 cm$^{-1}$ (for the most stable isomers). For $n = 14$, the absolute red shift with respect to the monomer is 217 cm$^{-1}$ (∼6.7%). This value is much larger than the usual shift observed for stable and unstable species in Ar matrixes (<2%).[74] This may indicate that the $\nu_3$ shift in $H_2O^+-Ar_n$ is far from being converged at $n = 14$ (owing to incomplete shielding of the positive charge) and further solvation shells may provide significant contributions to the $\nu_3$ shift of $H_2O^+$ embedded in an Ar matrix. Alternatively, the shift may be converged at $n = 14$; in this case the resulting large Ar matrix shift can be explained by the fact that the $H_2O^+$ ion can only exist as a stable, small, and distinct $H_2O^+-Ar_n$ unit within the Ar matrix. For example, considering the $n = 4$ complex as such a stable core, the shift of the $n = 14$ complex with respect to the $n = 4$ complex is less than 1% and compatible with typical Ar matrix shifts.[74] Similar models have been invoked to rationalize unusual large shifts of related $AH^+$ ions embedded in neon matrixes[75] and argon clusters.[14]

Previous mass spectra of $H_2O^+-Ar_n$ showed discontinuities in the intensity distribution which have been attributed to enhanced stabilities for certain cluster sizes:[21] $n = 9$ was observed to be a strong magic number, whereas $n = 3, 5, 7$, and 15 are weakly enhanced. In contrast, for $M^{\pm}-Ar_n$ with small closed-shell ions (e.g., $M^+ = Ar^+$),[76] magic numbers have been found for $n = 12$, corresponding to the first solvation shell with icosahedral structure.[77] Similarly, systematic band shifts observed in IR spectra of $AH^+-Ar_n$ (A = CO, N$_2$, SiO)[13–15] suggested that the first Ar solvation shell around these ions is also filled at $n = 12$ and composed of two staggered equatorial five-membered solvation rings around a linear Ar−AH$^+$−Ar trimer. In the latter cases, the linear closed-shell core ion is of similar size as Ar$^+$, so that the AH$^+$−Ar$_{12}$ geometries are slightly distorted icosahedrons with a nearly spherical (impurity) ion in the center. The fact that the mass spectra of $H_2O^+-Ar_n$ do not show the magic number $n = 12$ was taken as evidence that the Ar solvation process is different for $H_2O^+$.[21] In particular, the structure of the strongly magic $n = 9$ cluster was

suggested to have a geometry where all nine ligands are equivalently solvated around the central $H_2O^+$ ion. However, such an isotropic structure is difficult to rationalize considering the large anisotropy calculated for the $H_2O^+-Ar$ interaction potential.[12] Although the IR spectra in Figures 8 and 9 are clearly more sensitive to the structures of $H_2O^+-Ar_n$ than the mass spectra, it is difficult to infer more details of the cluster growth for clusters with $n \geq 5$ owing to the lack of reliable theoretical information.[12] The $H_2O^+-Ar_n$ spectra reveal noticeable discontinuities in the $\nu_3$ and $\nu_3 + \nu_s^a$ frequencies for $n = 6$ and 9 (for the most stable isomers, Figures 8 and 9). These discontinuities are not necessarily indicative of an enhanced or decreased stability of these specific cluster sizes (like magic numbers in mass spectra). In contrast, the observed frequency shifts are sensitive to the structures of the complexes and in particular to the influence of the Ar ligands on the strengths of the O—H ($\nu_3$) and H—Ar ($\nu_s^a$) bonds. Similar $\nu_3$ and $\nu_s^a$ shifts are expected for Ar ligands occupying equivalent positions within the complex.[14] For example, in $OCH^+-Ar_n$ the five Ar ligands in each of the two equatorial rings around the linear $OCH^+-Ar$ dimer core shift the A—H stretch frequency roughly by equal amounts in the same direction.[13] Clearly, the IR spectra reveal that the cluster growth in $H_2O^+-Ar_n$ is largely different from that in $Ar_n^{(+)}$ and $AH^+-Ar_n$ (A = CO, $N_2$). However, this result may be expected, as the calculated potential for the $H_2O^+-Ar$ interaction is rather different from the other $AH^+-Ar$ potentials; it has lower symmetry and larger angular anisotropy. Owing to the two main attractive centers (the two H-bound sites) and the open-shell character (giving rise to the attraction at the p-bound sites), $H_2O^+$ cannot be approximated by a spherical or cylindrical central ion within slightly distorted icosahedral-like $Ar_n$ clusters. A definitive assignment of the spectral features to the individual $H_2O^+-Ar_n$ isomers has, however, to await a reliable theoretical treatment of the larger clusters, which is beyond the scope of the present work. In neutral $H_2O-Ar$, the strength and anisotropy of the interaction is very weak compared with $H_2O^+-Ar$. Consequently, the larger $H_2O-Ar_n$ clusters are calculated to have icosahedral-like geometries (similar to $Ar_{n+1}$) with an almost spherical interior $H_2O$ impurity and first shell closure at $n = 12$.[78] Comparison between $NH_4^+-Ar_n$ and $H_2O^+-Ar_n$ reveals that in both cases Ar atoms are first attached to the protons forming equivalent H-bonds, whereas further ligands occupy less favorable binding sites.[18]

Photoexcitation of $H_2O^+-Ar_n$ parent complexes at their $\nu_3$ band maxima leads to the observation of several $H_2O^+-Ar_m$ ($m < n$) fragment channels (Table 4). For example, for $H_2O^+-Ar_4$ two fragment channels are evident: $H_2O^+-Ar_3$ ($\sim$80%) and $H_2O^+-Ar_2$ ($\sim$20%). Figure 8 shows the spectra recorded in the dominant fragment channels. They are in most cases very similar to the spectra obtained in the less probable channels. Similar to previous studies on related systems[13–16,18] the observed range of $m$ for a given $n$ is rather narrow (Table 4). This information can be used to estimate rough values for incremental binding energies, $D_0(n)$, within a statistical model that is based on the following approximations: (i) the difference in the internal energies of parent and daughter ions, as well as the kinetic energy release, is neglected; (ii) only Ar atoms and no Ar clusters are evaporated; (iii) Ar ligands with smaller binding energies are evaporated first. Based on these assumptions, the absorbed photon energy must be larger than the sum of the binding energies of the $(n - m)$ evaporated ligands, but smaller than the sum of the $(n - m + 1)$ most weakly bound ligands in the parent cluster. As further approximation, Ar

**TABLE 4: Photofragmentation Branching Ratios for the Reaction $H_2O^+-Ar_n + h\nu \rightarrow H_2O^+-Ar_m + (n-m)$ Ar, Measured at the Peak Maxima of the $\nu_3$ Bands of the Most Stable Isomers[a]**

| $n$ | 1 | 2 | 3 | 4 | 5 | 6 | 7 |
|---|---|---|---|---|---|---|---|
| $m$ | 0 (1.0) | 1 (1.0) | 2 (1.0) | 2 (0.8) | 3 (1.0) | 3 (0.5) | 4 (1.0) |
| | | | | 3 (0.2) | | 4 (0.2) | |
| | | | | | | 5 (0.3) | |
| $\langle n-m \rangle$ | 1.0 | 1.0 | 1.0 | 1.8 | 2.0 | 2.2 | 3.0 |

| $n$ | 8 | 9 | 10 | 11 | 12 | 13 |
|---|---|---|---|---|---|---|
| $m$ | 4 (1.0) | 5 (1.0) | 5 (1.0) | 6 (1.0) | 6 (0.2) | 6 (0.1) |
| | | | | | 7 (0.8) | 7 (0.45) |
| | | | | | | 8 (0.45) |
| $\langle n-m \rangle$ | 4.0 | 4.0 | 5.0 | 5.0 | 5.2 | 5.65 |

[a] The average number of Ar atoms lost, $\langle n-m \rangle$ is also given. Uncertainties are estimated as $\pm 0.05$. Channels contributing less than 5% are neglected.

ligands attached at similar binding sites are assumed to have the same binding energy (three-body effects are neglected). Based on the dimer PES calculated in article I,[12] the Ar ligands in $H_2O^+-Ar_n$ are classified into three groups: H-bound ($n = 1,2$), p-bound ($n = 3,4$) and other ligands ($n = 5-10$). Using the photofragmentation branching ratios in Table 4, the following limits are derived for the binding energies of the three classes: 1400 cm$^{-1}$ < $D_0(1,2)$ < 2800 cm$^{-1}$; 1100 cm$^{-1}$ < $D_0(3,4)$ < 1500 cm$^{-1}$; 600 cm$^{-1}$ < $D_0(5-10)$ < 750 cm$^{-1}$. These values compare favorably with the binding energies expected from the $H_2O^+-Ar$ PES: $D_0 = 2200$ cm$^{-1}$ for the H-bond and 1300 cm$^{-1}$ for the p-bond. Other binding sites are calculated to be less stable with binding energies between 350 and 1000 cm$^{-1}$. From Table 4 it is evident that the average number of Ar atoms lost upon $\nu_3$ excitation, $\langle n-m \rangle$, increases as a function of cluster size and is not converged at $n \sim 12$. This observation confirms the decrease in the incremental binding energy for increasing $n$, as the absorbed photon energy is roughly constant ($\nu_3 \sim 3000$ cm$^{-1}$).

For $n = 13$, the photofragmentation ratios of the two $\nu_3$ bands differ considerably. For the 3037 cm$^{-1}$ band the observed fragment distribution is $m = 6$ (10%), $m = 7$ (45%), and $m = 8$ (45%) giving rise to an average loss 5.65 Ar atoms. For the 3024 cm$^{-1}$ band the distribution is $m = 5$ (20%), $m = 6$ (20%), $m = 7$ (40%), and $m = 8$ (20%) yielding an average loss of 6.40 Ar atoms. The observation of largely different fragmentation behavior for two closely spaced bands confirms the conclusion above that the two bands arise from $\nu_3$ absorptions of two different isomers rather than from $\nu_1$ and $\nu_3$ bands of a single isomer. A similar strategy has been used recently to identify isomers of $H^+(CH_3OH)_4H_2O$.[79]

**References and Notes**

(1) Hobza, P.; Zahradnik, R. *Intermolecular Complexes: The Role of van der Waals Systems in Physical Chemistry and in the Biodisciplines*; Elsevier: Amsterdam, 1988.

(2) Marcus, Y. *Ion Solvation*; Wiley: New York, 1985.

(3) Castleman, A. W.; Keesee, R. G. *Chem. Rev.* **1986**, *86*, 589.

(4) Lifshitz, C. In *Cluster Ions*; Ng, C.-Y., Baer, T., Powis, I., Eds.; Wiley: New York, 1993.

(5) Keesee, R. G.; Castleman, A. W., Jr. *J. Phys. Chem. Ref. Data* **1986**, *15*, 1011.

(6) Bieske, E. J.; Maier, J. P. *Chem. Rev.* **1993**, *93*, 2603.

(7) Lisy, J. M. In *Cluster Ions*; Ng, C.-Y., Baer, T., Powis, I., Eds.; Wiley: New York, 1993.

(8) Bieske, E. J. *J. Chem. Soc., Faraday Trans.* **1995**, *91*, 1.

(9) Duncan, M. A. *Annu. Rev. Phys. Chem.* **1997**, *48*, 69.

(10) Bieske, E. J.; Dopfer, O. *Chem. Rev.* **2000**, *100*, 3963.

(11) Müller-Dethlefs, K.; Hobza, P. *Chem. Rev.* **2000**, *100*, 143.

(12) Dopfer, O. *J. Chem. Phys. A* **2000**, *104*, 11693.

(13) Nizkorodov, S. A.; Dopfer, O.; Ruchti, T.; Meuwly, M.; Maier, J. P.; Bieske, E. J. *J. Phys. Chem.* **1995**, *99*, 17118.

(14) Dopfer, O.; Olkhov, R. V.; Maier, J. P. *J. Phys. Chem. A* **1999**, *103*, 2982.

(15) Olkhov, R. V.; Nizkorodov, S. A.; Dopfer, O. *Chem. Phys.* **1998**, *239*, 393.

(16) Olkhov, R. V.; Nizkorodov, S. A.; Dopfer, O. *J. Chem. Phys.* **1998**, *108*, 10046.

(17) Bieske, E. J.; Nizkorodov, S. A.; Dopfer, O.; Maier, J. P.; Stickland, R. J.; Cotterell, B. J.; Howard, B. J. *Chem. Phys. Lett.* **1996**, *250*, 266.

(18) Dopfer, O.; Nizkorodov, S. A.; Meuwly, M.; Bieske, E. J.; Maier, J. P. *Int. J. Mass Spectrom. Ion Processes* **1997**, *167−168*, 637.

(19) Lakin, N. M.; Dopfer, O.; Meuwly, M.; Howard, B. J.; Maier, J. P. *Mol. Phys.* **2000**, *98*, 63.

(20) Lakin, N. M.; Dopfer, O.; Howard, B. J.; Maier, J. P. *Mol. Phys.* **2000**, *98*, 81.

(21) Vaidyanathan, G.; Coolbaugh, M. T.; Peifer, W. R.; Garvey, J. F. *J. Phys. Chem.* **1991**, *95*, 4193.

(22) Lew, H. *Can. J. Phys.* **1976**, *54*, 2028.

(23) Roth, D.; Nizkorodov, S. A.; Maier, J. P.; Dopfer, O. *J. Chem. Phys.* **1998**, *109*, 3841.

(24) Dopfer, O.; Nizkorodov, S. A.; Olkhov, R. V.; Maier, J. P.; Harada, K. *J. Phys. Chem. A* **1998**, *102*, 10017.

(25) Dopfer, O.; Roth, D.; Maier, J. P. *Chem. Phys. Lett.* **1999**, *310*, 201.

(26) Dopfer, O.; Olkhov, R. V.; Roth, D.; Maier, J. P. *Chem. Phys. Lett.* **1998**, *296*, 585.

(27) Dopfer, O.; Roth, D.; Maier, J. P. *J. Chem. Phys.* **2000**, *113*, 120.

(28) Kapras, Z.; Huntress Jr, W. T. *Chem. Phys. Lett.* **1978**, *59*, 87.

(29) Anicich, V. G. *J. Chem. Phys. Ref. Data* **1993**, *22*, 1469.

(30) Brundle, C. R.; Turner, D. W. *Proc. R. Soc. London* **1968**, *A 307*, 27.

(31) Reutt, J. E.; Wang, L. S.; Lee, Y. T.; Shirley, D. A. *J. Chem. Phys.* **1986**, *85*, 6928.

(32) Tonkyn, R. G.; Wiedmann, R.; Grant, E. R.; White, M. G. *J. Chem. Phys.* **1991**, *95*, 7033.

(33) Merkt, F.; Signorell, R.; Palm, H.; Osterwalder, A.; Sommavilla, M. *Mol. Phys.* **1998**, *95*, 1045.

(34) Strahan, S. E.; Mueller, R. P.; Saykally, R. J. *J. Chem. Phys.* **1986**, *85*, 1252.

(35) Liu, D.-J.; Ho, W.-C.; Oka, T. *J. Chem. Phys.* **1987**, *87*, 2442.

(36) Mürtz, P.; Zink, L. R.; Evenson, K. M.; Brown, J. M. *J. Chem. Phys.* **1998**, 9744.

(37) Dinelli, B. M.; Crofton, M. W.; Oka, T. *J. Mol. Spectrosc.* **1988**, *127*, 1.

(38) Brown, P. R.; Davies, P. B.; Stickland, R. J. *J. Chem. Phys.* **1989**, *91*, 3384.

(39) Huet, T. R.; Pursell, C. J.; Ho, W. C.; Dinelli, B. M.; Oka, T. *J. Chem. Phys.* **1992**, *97*, 5977.

(40) Das, B.; Farley, J. W. *J. Chem. Phys.* **1991**, *95*, 8809.

(41) Huet, T. R.; Bachir, H.; Destombes, J. L.; Vervloet, M. *J. Chem. Phys.* **1997**, *107*, 5645.

(42) Forney, D.; Jacox, M. E.; Thompson, W. E. *J. Chem. Phys.* **1993**, *98*, 841.

(43) Jackels, C. F. *J. Chem. Phys.* **1980**, *72*, 4873.

(44) Botschwina, P. Habilitation thesis, Universität Kaiserslautern, 1984.

(45) Degli Esposti, A.; Lister, D. G.; Palmieri, P.; Degli Esposti, C. *J. Chem. Phys.* **1987**, *87*, 6772.

(46) Botschwina, P. In *Ion and Cluster Ion Spectroscopy and Structure*; Maier, J. P., Ed.; Elsevier: Amsterdam, 1989.

(47) Weis, B.; Carter, S.; Rosmus, P.; Werner, H. J.; Knowles, P. J. *J. Chem. Phys.* **1989**, *91*, 2818.

(48) Weis, B.; Yamashita, K. *J. Chem. Phys.* **1993**, *99*, 9512.

(49) Brommer, M.; Weis, B.; Follmeg, B.; Rosmus, P.; Carter, S.; Handy, N. C.; Werner, H. J.; Knowles, P. J. *J. Chem. Phys.* **1993**, *98*, 5222.

(50) Lopez, G. E. *J. Comput. Chem.* **1995**, *16*, 768.

(51) Shinohara, H.; Nishi, N.; Washida, N. *J. Chem. Phys.* **1986**, *84*, 5561.

(52) Shiromaru, H.; Shinohara, H.; Washida, N.; Yoo, H.-S.; Kimura, K. *Chem. Phys. Lett.* **1987**, *141*, 7.

(53) Tomoda, S.; Kimura, K. In *Photoionization and Photodissociation of Small Molecules and Clusters*; Ng, C. Y., Ed.; World Scientific: Singapore, 1992.

(54) Norwood, K.; Ali, A.; Ng, C. Y. *J. Chem. Phys.* **1991**, *95*, 8029.

(55) Guelachvili, G.; Rao, K. N. *Handbook of Infrared Standards*; Academic Press: London, 1993.

(56) Herzberg, G. *Molecular Spectra and Molecular Structure. II. Infrared and Raman Spectra of Polyatomic Molecules*; Krieger Publishing Company: Malabar, FL, 1991.

(57) Raynes, W. T. *J. Chem. Phys.* **1964**, *41*, 3020.

(58) Olkhov, R. V.; Nizkorodov, S. A.; Dopfer, O. *J. Chem. Phys.* **1997**, *107*, 8229.

(59) Bumgarner, R. E.; Suzuki, S.; Stockman, P. A.; Green, P. G.; Blake, G. A. *Chem. Phys. Lett.* **1991**, *176*, 123.

(60) Crofton, M. W.; Altman, R. S.; Jagod, M.-F.; Oka, T. *J. Phys. Chem.* **1985**, *89*, 3614.

(61) Meot-Ner, M. *J. Am. Chem. Soc.* **1984**, *106*, 1257.

(62) Pimentel, G. C.; McClellan, A. L. *The Hydrogen Bond*; Freeman: London, 1960.

(63) Miller, R. E. *Acc. Chem. Res.* **1990**, *23*, 10.

(64) Le Roy, R. J.; Davies, M. R.; Lam, M. E. *J. Phys. Chem.* **1991**, *95*, 2167.

(65) Okumura, M.; Yeh, L. I.; Myers, J. D.; Lee, Y. T. *J. Phys. Chem.* **1990**, *94*, 3416.

(66) Dopfer, O.; Roth, D.; Olkhov, R. V.; Maier, J. P. *J. Chem. Phys.* **1999**, *110*, 11911.

(67) Dopfer, O. et al., unpublished results.

(68) Bogey, M.; Bolvin, H.; Demuynck, C.; Destombes, J. L.; Van Eijck, B. P. *J. Chem. Phys.* **1988**, *88*, 4120.

(69) Nizkorodov, S. A.; Dopfer, O.; Meuwly, M.; Maier, J. P.; Bieske, E. J. *J. Chem. Phys.* **1996**, *105*, 1770.

(70) Cohen, R. C.; Saykally, R. J. *J. Chem. Phys.* **1993**, *98*, 6007.

(71) Lascola, R.; Nesbitt, D. J. *J. Chem. Phys.* **1991**, *95*, 7917.

(72) Weida, M. J.; Nesbitt, D. J. *J. Chem. Phys.* **1997**, *106*, 3078.

(73) Hutson, J. M. *Annu. Rev. Phys. Chem.* **1990**, *41*, 123.

(74) Jacox, M. E. *Chem. Phys.* **1994**, *189*, 149.

(75) Lugez, C. L.; Jacox, M. E.; Johnson III, R. D. *J. Chem. Phys.* **1999**, *110*, 5037.

(76) Harris, I. A.; Kidwell, R. S.; Northby, J. A. *Phys. Rev. Lett.* **1984**, *53*, 2390.

(77) Mackay, A. L. *Acta Crystallogr.* **1962**, *15*, 916.

(78) Liu, S. Y.; Bacic, Z.; Moskowitz, J. W.; Schmidt, K. E. *J. Chem. Phys.* **1994**, *101*, 8310.

(79) Chaudhuri, C.; Jiang, J. C.; Wang, X.; Lee, Y. T.; Chang, H.-C. *J. Chem. Phys.* **2000**, *112*, 7279.

(80) Hunter, E. P. L.; Lias, S. G. *J. Phys. Chem. Ref. Data* **1998**, *27*, 413.

(81) Huntress, W. T. *Astrophys. J. Suppl.* **1977**, *33*, 495.

(82) Nizkorodov, S. A.; Spinelli, Y.; Bieske, E. J.; Maier, J. P.; Dopfer, O. *Chem. Phys. Lett.* **1997**, *265*, 303.

(83) Botschwina, P.; Oswald, R.; Linnartz, H.; Verdes, D. *J. Chem. Phys.* **2000**, *113*, 2736.